



# Photocatalytic performance improvement by utilizing GO\_MWCNTs hybrid solution on sand/ZnO/TiO<sub>2</sub>-based photocatalysts to degrade methylene blue dye

Nur Jannah Idris<sup>1,2</sup> · Suriani Abu Bakar<sup>1,2</sup> · Azmi Mohamed<sup>1,3</sup> · Muqoyyanah Muqoyyanah<sup>1,2</sup> · Mohd Hafiz Dzarfan Othman<sup>4</sup> · Mohamad Hafiz Mamat<sup>5</sup> · Mohd Khairul Ahmad<sup>6</sup> · Muhammad Danang Birowosuto<sup>7</sup> · Tetsuo Soga<sup>8</sup>

Received: 20 April 2020 / Accepted: 16 September 2020 / Published online: 6 October 2020  
© Springer-Verlag GmbH Germany, part of Springer Nature 2020

## Abstract

In this work, sand/zinc oxide (ZnO)/titanium dioxide (TiO<sub>2</sub>)-based photocatalysts were hybridized with graphene oxide (GO) and GO\_multi-walled carbon nanotubes (MWCNTs) hybrid solution. The novel hybrid was then used in photocatalysis to degrade dye contamination. The nanocomposite photocatalyst was initially fabricated by growing ZnO nanorods (NRs) via sol-gel immersion followed by synthesizing TiO<sub>2</sub> NRs for different times (5 and 20 h) using a hydrothermal method on sand as a substrate. Prior to the hybridization, the initial GO was synthesized using electrochemical exfoliation and further mixed with 1 wt% MWCNTs to form GO\_MWCNTs hybrid solution. The synthesized GO and GO\_MWCNTs hybrid solution were then incorporated onto sand/ZnO/TiO<sub>2</sub> nanocomposite-based photocatalysts through immersion. Various sand/ZnO/TiO<sub>2</sub>-based photocatalysts were then tested for methylene blue (MB) dye degradation within 3 days. On the basis of UV-Vis measurement, the highest MB degradation was achieved by using sand/ZnO NRs/TiO<sub>2</sub> NRs (5 h)/GO\_MWCNTs (92.60%). The high surface area and high electrical conductivity of GO\_MWCNTs prolonged the lifetime of electron/hole separation and thus enhanced the photocatalytic performance.

**Keywords** Sand · ZnO · TiO<sub>2</sub> · GO\_MWCNTs · Photocatalysis · Dye

## Introduction

Nowadays, clean water sources are limited due to the pollution from industries which release waste disposal into fresh

water sources without proper treatment. Textile wastewater contains various heavy metals and non-biodegradable organic dyes, which pose a serious problem for human health and the environment (Saravanan et al. 2017). Furthermore, most

---

Responsible Editor: Sami Rtimi

---

✉ Suriani Abu Bakar  
absuriani@yahoo.com

<sup>1</sup> Nanotechnology Research Centre, Faculty of Science and Mathematics, Universiti Pendidikan Sultan Idris, 35900 Tanjung Malim, Perak, Malaysia

<sup>2</sup> Department of Physics, Faculty of Science and Mathematics, Universiti Pendidikan Sultan Idris, 35900 Tanjung Malim, Perak, Malaysia

<sup>3</sup> Department of Chemistry, Faculty of Science and Mathematics, Universiti Pendidikan Sultan Idris, 35900 Tanjung Malim, Perak, Malaysia

<sup>4</sup> Advanced Membrane Technology Research Centre (AMTEC), Universiti Teknologi Malaysia, 81310 Skudai, Johor, Malaysia

<sup>5</sup> NANO-ElecTronic Centre (NET), Faculty of Electrical Engineering, Universiti Teknologi MARA (UiTM), 40450 Shah Alam, Selangor, Malaysia

<sup>6</sup> Microelectronic and Nanotechnology-Shamsuddin Research Centre (MiNT-SRC), Faculty of Electrical and Electronic Engineering, Universiti Tun Hussein Onn Malaysia, Parit Raja, Malaysia

<sup>7</sup> CNRS International NTU Thales Research Alliance (CINTRA), Research Techno Plaza, 50 Nanyang Drive, Border X Block, Singapore 637553, Singapore

<sup>8</sup> Department of Frontier Materials, Nagoya Institute of Technology, Gokiso-cho, Showa-ku, Nagoya 466-8555, Japan

organic dyes are rich in hazardous chemicals which are difficult to remove (Katheresan et al. 2018; Maučec et al. 2018). Methylene blue (MB) is an organic dye that is difficult to decompose because of its complex aromatic structure (Sun et al. 2018). Water mixed with MB dye is difficult to treat and decolorize (Basturk and Karatas 2015). Therefore, methods to degrade MB need to be developed to obtain clean and fresh water. Photocatalysis is an efficient and environment-friendly process for dye degradation and water purification (Khojasteh et al. 2018).

Zinc oxide (ZnO) is an ideal semiconductor photocatalyst owing to its high electron mobility (Qi et al. 2017), mechanical–thermal stability, high quantum efficiency, high photostability (Kumar and Rao 2015), good oxidizing power (Adnan et al. 2016) and high surface area (Liu et al. 2018). However, the agglomeration between ZnO particles decreases the number of active surface sites (Azmina et al. 2017) and thus weakens its photocatalytic performance. In addition, ZnO photocatalyst is inefficient in powder form because it disperses in water and produces a milky solution, which hinders photocatalyst activation under UV light (Eddy et al. 2015). A substrate is clearly needed to activate the photocatalyst (Alansi et al. 2015; Fadillah et al. 2019; Saleh 2020) and perform photocatalysis. Substrates usually used in photocatalysis are clay, glass, zeolite, silica, sand and fly ash. Sand offers several advantages, such as porous morphology, high density, local availability, low cost and chemical inertness (Abdel-Maksoud et al. 2018; Hadjitaief et al. 2016; Shan et al. 2010).

Given its broad band gap energy (3.37 eV), ZnO also possesses a limitation in photocatalysis because the high recombination rate between electron–hole pairs could affect the photocatalytic performance (Hellen et al. 2018; Sun et al. 2018). Therefore, ZnO photocatalyst must be composited with other semiconductor, metal, non-metal or carbon-based materials to overcome this limitation (Banerjee et al. 2018; Sun et al. 2018). Semiconductor–semiconductor composites such as ZnO/titanium dioxide (TiO<sub>2</sub>) show excellent photocatalytic performance (Cheng et al. 2014; Habib et al. 2013). The lifetime of the photogenerated electron/hole is prolonged when ZnO and TiO<sub>2</sub> are composited because TiO<sub>2</sub> acts as a trap site which prevents electron–hole recombination (Hadjitaief et al. 2016; Hellen et al. 2018). Moreover, the incorporation of ZnO into TiO<sub>2</sub> can decrease the band gap value and extend the light absorption range (Bai et al. 2013; Cirak et al. 2018; Wetchakun et al. 2019). Cirak et al. (2018) showed that compositing ZnO and TiO<sub>2</sub> achieves 95% dye degradation, which is higher than that obtained by pure TiO<sub>2</sub> photocatalyst (65%). In addition, Cheng et al. (2014, 2016) showed that ZnO/TiO<sub>2</sub> nanocomposites perform higher photocatalytic activity than pure ZnO and TiO<sub>2</sub>. These results agree with the report of Hadjitaief et al. (2016) that ZnO/TiO<sub>2</sub>/clay nanocomposites achieve a higher dye degradation of 98.7% than TiO<sub>2</sub>/clay (87.2%).

Several methods are used to synthesize ZnO, TiO<sub>2</sub> and their nanocomposite. Sol–gel and hydrothermal methods offer uniform size distribution, various morphologies (Ba-abbad et al. 2013), low temperature operation, simple procedures (Ong et al. 2018) and high purity and crystallinity (Ong et al. 2018; Wetchakun et al. 2019) of nanocomposites. The sol–gel method also promotes good purity, dispersion and homogeneity (Bodson et al. 2010). Cheng et al. (2016) synthesized ZnO/TiO<sub>2</sub> nanocomposites by using a two-step hydrothermal method and achieved the complete degradation of methylene orange (MO) dye within 25 min. Siwińska-Stefańska et al. (2019) fabricated TiO<sub>2</sub>/ZnO by using a hydrothermal method and exhibited high photocatalytic performance in removing C.I. Basic Violet 10 (95%) within 180 min. Earlier, Siwińska-Stefańska et al. (2018) synthesized TiO<sub>2</sub>/ZnO nanocomposites by using the sol–gel method and successfully degraded 93.4% of C.I. Basic Violet 10 dye within 120 min. Hakki et al. (2019) also synthesized TiO<sub>2</sub>/ZnO on glass by using sol–gel and dip-coating method and effectively removed 97.3% MB dye within 360 min.

Photocatalysts were also hybridized with carbon-based materials, such as graphene oxide (GO) and GO-multi-walled carbon nanotubes (MWCNTs) with large surface area (Saleh 2011; Saleh 2015a, b, c) and high electron mobility to enhance their performance (Mahmoodi 2013; Saleh 2013; Tayel et al. 2018). The utilization of GO and MWCNTs onto the photocatalyst further improves photocatalysis (Da Dalt et al. 2016; Zhang et al. 2016). Chaudhary et al. (2018) showed that ZnO/MWCNTs achieve 93% of MB degradation, whereas pure ZnO can only reach 48%. Meanwhile, Raliya et al. (2017) showed that the hybridization of GO with TiO<sub>2</sub>/ZnO nanocomposites enhances the photocatalytic performance from 40 to 44%. These results agree with the finding of Da Dalt et al. (2016) that the incorporation of MWCNTs with TiO<sub>2</sub>/ZnO achieves higher photocatalytic activity than TiO<sub>2</sub>/ZnO nanocomposites.

High-quality GO is commonly synthesized via Hummers' method (Kumar et al. 2010). However, this method presents several drawbacks, such as the utilization of hazardous chemicals that can damage the environment, require several procedures and entail long production time (Brodie 1859; Hummers and Offeman 1957). A simpler electrochemical exfoliation becomes a promising method to synthesize GO in large-scale production (Md Disa et al. 2015; Wu et al. 2017; Yu et al. 2015). In addition, the utilization of water-based electrolytes with the assistance of a surfactant for GO layer intercalation offers environment-friendly, economic and less hazardous chemical usage (Md Disa et al. 2015; Suriani et al. 2018a, b, c).

GO-based materials can be transferred onto ZnO/TiO<sub>2</sub> nanocomposites via spray coating, spin coating, dip coating and immersion. Spray coating is simple and provides a large surface area coverage onto the desired substrate (Liu 2017;

Chen et al. 2018). However, the uniformity of the coverage is relatively poor, and material wastage or loss occurs during the process (Liu 2017). Moreover, this method requires expensive apparatus. Meanwhile, dip coating possesses a slow coating process. Spin coating is easy to handle, is cheap and provides high uniformity. However, it also results in coating material wastage, produces a non-uniform layer and is only suitable for flat substrates. By contrast, immersion offers a simple, low-cost (Poorebrahimi and Norouzbeigi 2015) and time-saving method (Latthe et al. 2012), which is suitable for large-scale production and facilitates homogenous coating over the substrate.

The method to synthesize ZnO/TiO<sub>2</sub> nanocomposite by combining sol–gel immersion and hydrothermal method is not well explored. In addition, the utilization of immersion method to transfer GO-based materials onto the ZnO/TiO<sub>2</sub> nanocomposite is also rarely explored. Therefore, in the present work, the photocatalyst materials were fabricated by combining ZnO, TiO<sub>2</sub>, GO and MWCNTs on sand substrate. The novel combination of ZnO and TiO<sub>2</sub> synthesized by sol–gel immersion and hydrothermal method, respectively, prior to the hybridization with GO-based materials using immersion was used as a sand-based photocatalyst in MB dye degradation. To the best of our knowledge, the novelty of this study lies on the utilization of sand/ZnO/TiO<sub>2</sub>-based photocatalysts hybridized with GO synthesized by electrochemical exfoliation and MWCNTs synthesized from waste cooking palm oil.

## Experimental and methods

### Materials

Sand, zinc nitrate (Zn(NO<sub>3</sub>)<sub>2</sub>) and hexamethylenetetramine (HMT) were used for sand/ZnO NRs synthesis. Titanium butoxide (TBOT) (Sigma-Aldrich) and hydrochloric acid (HCl, 36.5–38% concentration, JT Baker) were used for TiO<sub>2</sub> NR synthesis. Graphite rods (99.99%, 150 mm in length and 10 mm in diameter, GoodFellow GmbH, Germany) and a commercially available sodium dodecyl sulphate (SDS) (Sigma-Aldrich) surfactant were used in GO synthesis. MWCNTs from waste cooking palm oil were used to prepare GO\_MWCNTs hybrid solution. Meanwhile, the MB dye (Sigma-Aldrich) was used for dye degradation test.

### Fabrication of sand/ZnO NRs

A 0.05 M ZnO solution was prepared by dissolving 1.407 g of HMT and 2.975 g of zinc nitrate into 200 mL of DI water in a Schott-capped bottle. The prepared solution was then sonicated in an ultrasonic cleaner for 30 min at 50 °C prior to stirring for 2 h at room temperature. The obtained solution was then left for 1 day at room temperature for aging. The prepared

solution was separated equally into two Schott-capped bottles and then added with 25 g of sand. The Schott-capped bottles were placed into a water bath to perform the sol–gel synthesis for 4 h at 95 °C. The sand was then removed and rinsed with DI water and directly dried for 10 min in an electric oven at 150 °C. The dried sand was further annealed for 1 h at 500 °C.

### Fabrication of sand/ZnO/TiO<sub>2</sub> nanocomposite

A sand/ZnO/TiO<sub>2</sub> nanocomposite was prepared by growing TiO<sub>2</sub> NRs on the fabricated sand/ZnO using a hydrothermal method. Hydrothermal solution was prepared by mixing 60 mL of DI water and 60 mL of HCl for about 5 min. Next, 3 mL of TBOT was added into the solution dropwise and stirred for another 15 min until a clear solution was observed. The prepared hydrothermal solution was poured into an autoclave followed by 40 g of the synthesized sand/ZnO NRs. The autoclave was then heated in an electric oven for 5 and 20 h at 150 °C to perform hydrothermal synthesis. The autoclave was directly taken out and allowed to cool down at room temperature. The synthesized sand/ZnO NRs/TiO<sub>2</sub> was then taken out and rinsed using DI water. The sample was heated in an electric oven for 5 min at 150 °C and then annealed for 1 h at 400 °C.

### Synthesis of graphene oxide

GO was synthesized by electrochemical exfoliation as previously described (Md Disa et al. 2015; Suriani et al. 2018a, b, c). Two graphite rods were partially immersed into 0.1 M of electrolyte containing SDS surfactant and connected to the DC power supply (7 V) for 24 h at room temperature.

### Preparation of GO\_MWCNTs hybrid solution

The MWCNTs were prepared as previously described (Suriani et al. 2016). A hybrid solution of GO\_MWCNTs was prepared by mixing 1 wt% MWCNTs into the prepared GO solution with stirring for 1 h at room temperature to ensure that the MWCNTs were well dispersed in the GO solution (Suriani et al. 2018c; Suriani et al. 2019).

### Fabrication of sand/ZnO/TiO<sub>2</sub>/GO and ZnO/TiO<sub>2</sub>/GO\_MWCNTs nanohybrids

A total of 30 g of the fabricated sand/ZnO/TiO<sub>2</sub> was initially immersed in 30 mL of GO and GO\_MWCNTs hybrid solution and heated for 2 h at 90 °C on a hot plate. The nanohybrid photocatalysts were then annealed in an argon gas furnace at 400 °C for 1 h.

## Photocatalytic test

A photocatalysis test for MB degradation was performed under the illumination of UV light by utilizing 5 ppm MB. The MB solution was placed in a container followed by adding 30 g of photocatalyst. The container was then exposed under UV light irradiation for 3 days. The samples were taken daily for 3 days, and the MB concentration was determined by using UV-Vis. The photodegradation efficiency ( $\eta$ ) was calculated using the following equation:

$$\eta = \frac{[(c_0 - c_t)]}{c_0} \times 100\% \quad (1)$$

where  $C_0$  and  $C_t$  are the initial and specific times of MB concentration, respectively.

## Instrument and tools

The fabricated sand/ZnO/TiO<sub>2</sub>-based photocatalysts were characterized based on its morphological, structural and optical properties. The morphological and structural properties were observed by field emission scanning electron microscope (FESEM) instrument (Hitachi SU8020) and (ZEISS), energy dispersive X-ray (EDX) spectroscopy (Horiba EMAX) and micro-Raman spectroscopy (Renishaw InVia microRaman System). Meanwhile, the optical properties were measured by UV-Vis spectroscopy (Agilent Cary 60).

## Results and discussion

### FESEM and EDX analyses

The surface morphology of all fabricated sand/ZnO/TiO<sub>2</sub>-based photocatalysts was determined by FESEM, and the results are presented in Fig. 1. First sample of sand/ZnO NRs/TiO<sub>2</sub> NRs (5 h) showed a random arrangement with a low density of ZnO NRs and TiO<sub>2</sub> NRs (5 h) formation on the sand substrate (Fig. 1a). At high magnification, the synthesized TiO<sub>2</sub> NRs (5 h) possessed two pyramidal ends (see yellow arrows), whereas the ZnO NRs showed flat ends (see red arrows) (Fig. 1b). The pyramidal ends of TiO<sub>2</sub> NRs (5 h) were due to the presence of HCl, which decreased the surface energy of the NR plane side walls and resulted in anisotropic growth in the (101) direction (Mali et al. 2011). Meanwhile, the flat ends of ZnO NRs resulted from the dominant dissolution effect on the top of the (0001) surfaces due to the reduction in Zn(NH<sub>3</sub>)<sub>4</sub><sup>2+</sup> concentration (Wei et al. 2006).

The hydrolysis process of Zn(NO<sub>3</sub>)<sub>2</sub> and HMT produced Zn<sup>2+</sup> and OH<sup>-</sup>, which proposed the growth mechanism of ZnO NRs (Malek et al. 2015). The formation of ZnO nuclei was

obtained when the ZnO solution reached the supersaturation state, which then triggered the Zn<sup>2+</sup> to be reacted with OH<sup>-</sup> ions. As a consequence, the formation of ZnO nuclei on the sand substrate would initiate the growth of the ZnO NRs (4 h) (Malek et al. 2015). Four-hour growth time of ZnO NRs was found to be an optimal synthesis time in order to form the NRs nanostructure (Ridhuan et al. 2012). This result was in a good agreement with Fudzi et al. (2018), which confirmed that 4-h growth time was an optimum condition to grow ZnO NRs. Meanwhile, the formation of TiO<sub>2</sub> NRs is initiated with hydrolysis process where the H<sup>+</sup> ions from water molecules are captivated to the oxide ion of titanium butoxide (Ti(RO<sub>4</sub>)) (Arthi 2016). The OH<sup>-</sup> ions replaced the butyl groups (R) in (Ti(RO<sub>4</sub>)) and became Ti-OH groups (Arthi 2016; Prathan et al. 2020). Consequently, these processes resulted in the change of coordination number of Ti precursor (Ti(RO<sub>4</sub>)) from Ti<sup>4+</sup> to Ti<sup>6+</sup>. Under high pressure in the hydrothermal process, Ti<sup>6+</sup> transformed into octahedra followed by the formation of precipitate crystal.

The low growth density of the ZnO NRs/TiO<sub>2</sub> NRs (5 h) on the sand substrate was due to the utilization of HCl, which dissolved the initial amount of ZnO NRs and interrupted the growth of TiO<sub>2</sub> NRs (5 h). The ZnO NRs were slowly dissolved and released Zn<sup>2+</sup> ions, which then reacted with Cl<sup>-</sup> ions in the hydrothermal solution when interacted with a strong acid such as HCl. Meanwhile, the H<sup>+</sup> reacted with O<sup>2-</sup> and formed H<sub>2</sub>O (Greenwood and Earnshaw 1997). This process led to the reduction of Cl<sup>-</sup> and H<sup>+</sup> ions in the hydrothermal solution, which is responsible for the growth of TiO<sub>2</sub> NRs (5 h). In turn, the reduction of Cl<sup>-</sup> ions led to titanium precursor precipitation, which suppressed TBOT hydrolysis to form TiO<sub>2</sub> NRs (Liu and Aydil 2009) and thus resulted in the low density formation of TiO<sub>2</sub> NRs (5 h) (Fig. 1c, d). As shown in Fig. 1c, the low atomic percentages of Ti (1.2%) and Zn (0.7%) confirmed the low existence of both materials in the sand/ZnO NRs/TiO<sub>2</sub> NRs (5 h) nanocomposite. Moreover, the length and diameter of ZnO NRs and TiO<sub>2</sub> NRs (5 h) in the sand/ZnO NRs/TiO<sub>2</sub> NRs (5 h) nanocomposite ranged within 487 nm–1.9 μm and 181–466 nm and within 1–1.8 μm and 112–186 nm, respectively.

Lower ZnO NRs and TiO<sub>2</sub> NRs (20 h) density formation was observed on the sand/ZnO NRs/TiO<sub>2</sub> NRs (20 h) than on the sand/ZnO NRs/TiO<sub>2</sub> NRs (5 h) (Fig. 1d, e). The unobservable ZnO NRs were due to the dissolution of ZnO NRs in the hydrothermal solution (Greenwood and Earnshaw 1997). Prolonged interaction between ZnO NRs and HCl causes a high dissolution of ZnO NRs (Kalpana and Rajeswari 2018) and retains low amounts of Cl<sup>-</sup> and H<sup>+</sup> ions in the hydrothermal solution. As a consequence, lower ZnO and TiO<sub>2</sub> NRs (20 h) were observed in the sand/ZnO NRs/TiO<sub>2</sub> NRs (20 h) than in the sand/ZnO NRs/TiO<sub>2</sub> NRs (5 h). This result was supported by the EDX analysis result (Fig. 1f), i.e., low Ti atomic percentage (1.0%) and absence of Zn (0%). Meanwhile, the



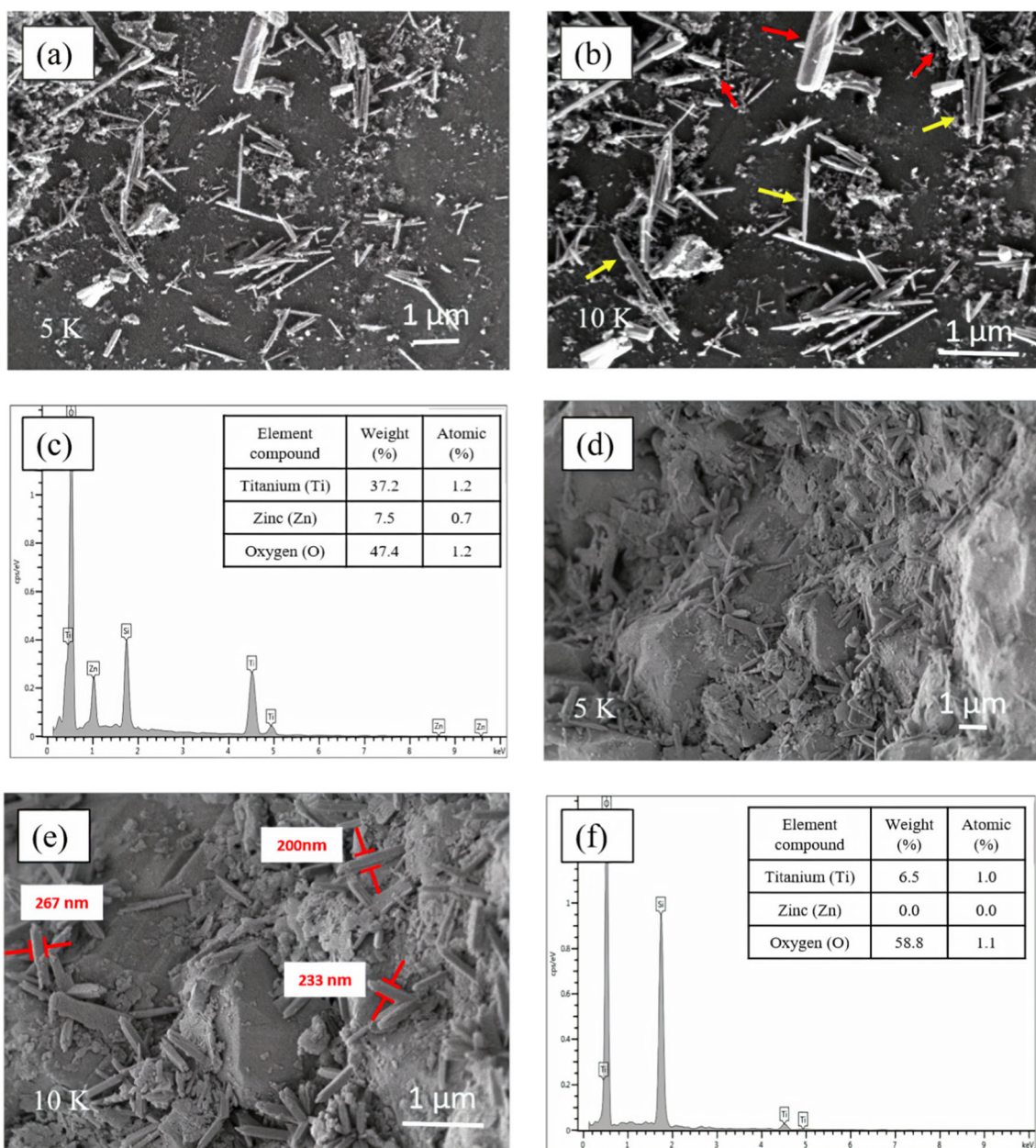


**Fig. 1** FESEM images with different magnification ranging between 5 and 50K X and EDX analysis of **a–c** sand/ZnO NRs/TiO<sub>2</sub> NRs (5 h), **d–f** sand/ZnO NRs/TiO<sub>2</sub> NRs (20 h), **g–i** sand/ZnO NRs/TiO<sub>2</sub> NRs (5 h)/GO and **j–l** sand/ZnO NRs/TiO<sub>2</sub> NRs (5 h)/GO\_MWCNTs

length and diameter of the TiO<sub>2</sub> NRs (20 h) in the sand/ZnO NRs/TiO<sub>2</sub> NRs (20 h) nanocomposite were 0.73–1.66 μm and 200–267 nm, respectively, compared with those in the sand/ZnO NRs/TiO<sub>2</sub> NRs (5 h).

The morphologic structures of the sand/ZnO NRs/TiO<sub>2</sub> NRs (5 h)/GO and sand/ZnO NRs/TiO<sub>2</sub> NRs (5 h)/GO\_MWCNTs nanohybrid are presented in Fig. 1g–l. As shown in Fig. 1g, h, GO sheets were homogeneously covered on top of the TiO<sub>2</sub> NRs (5 h) (white arrows) in the sand/ZnO NRs/TiO<sub>2</sub> NRs (5 h)/GO sample. The interaction between GO sheets and MWCNTs tube walls can be considered as a three-dimensional sheet and tube structure (Min et al. 2018). The

hydroxyl groups of TiO<sub>2</sub> NRs (5 h) interacted with the oxygen functional groups of GO forming Ti-O-C by hydrogen bonds, which resulted in homogeneity of GO on the TiO<sub>2</sub> NRs (5 h) (Naknikham et al. 2017; Qiu et al. 2012; Yu et al. 2017). EDX analysis of the sand/ZnO NRs/TiO<sub>2</sub> NRs (5 h)/GO presented 7.0%, 0.9% and 4.4% atomic percentages, which represented Ti, Zn and C, respectively (Fig. 1i). The morphology of the sand/ZnO NRs/TiO<sub>2</sub> NRs (5 h)/GO\_MWCNTs showed bundles of thread-like MWCNTs, which were well dispersed on the sand/ZnO NRs/TiO<sub>2</sub> NRs (5 h) nanocomposite (Fig. 1j, k). The average diameter of the MWCNTs was observed in the range of 50.2–92.1 nm, which was in a good agreement with

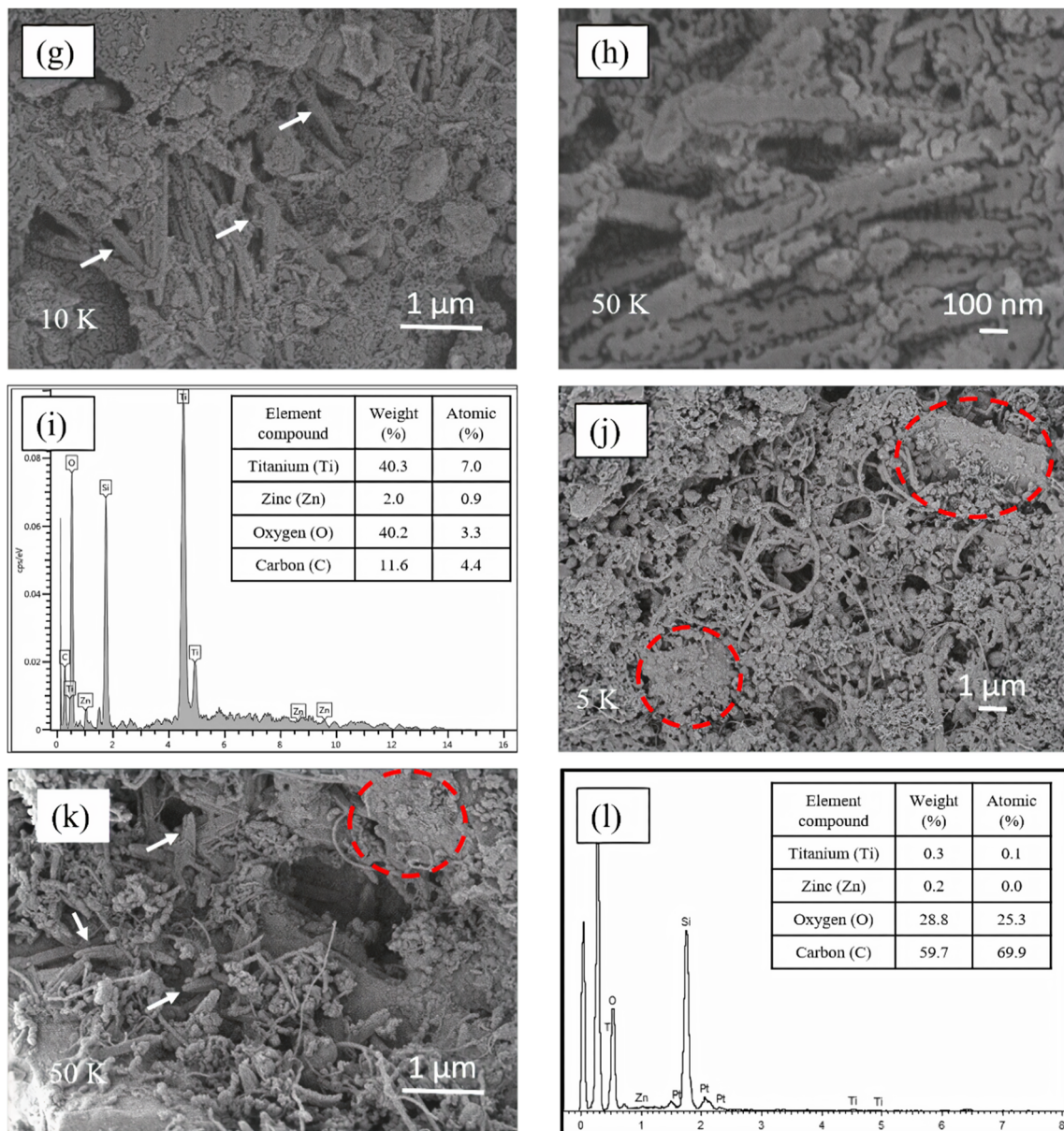


Fig. 1 (continued)

the previous work (Suriani et al. 2018c). The MWCNTs possessed smooth surface which bound and entangled toward each other. These MWCNTs were wrapped and strongly stacked on the GO sheets.

Moreover, the GO sheets (see red circle) were well adsorbed and dispersed between the MWCNTs emptiness due to the interactions between the side walls of the MWCNTs and hydrophobic region of the GO (Fig. 1j, k) (Shahriary et al. 2014). The weak  $\pi$ - $\pi$  stacking interactions between GO and MWCNTs could prevent the MWCNTs from aggregating with each other and provide higher surface area as compared with individual GO or MWCNTs (Chen et al. 2018; Zhang et al. 2010). The tetragonal structure of TiO<sub>2</sub> NRs (5 h) with two pyramidal ends (white arrows) under

the bundles of MWCNTs is shown in Fig. 1k. The higher atomic percentage of C (69.89%) in the sand/ZnO NRs/TiO<sub>2</sub> NRs (5 h)/GO\_MWCNTs than in the sand/ZnO NRs/TiO<sub>2</sub> NRs (5 h)/GO (4.4%) was due to the high content of C contributed by the incorporation of MWCNTs (Fig. 1l).

### Micro-Raman spectroscopy

Micro-Raman spectroscopy was carried out to investigate the crystallinity of the fabricated sand/ZnO/TiO<sub>2</sub>-based photocatalyst materials. The micro-Raman spectra of sand/ZnO NRs/TiO<sub>2</sub> NRs (5 and 20 h) showed five peaks in the range of 100–800 cm<sup>-1</sup>, as presented in Fig. 2. On the basis of the Raman spectra, the sand/ZnO NRs/TiO<sub>2</sub> NRs (5 h)



nanocomposite (black line graph) showed a weak peak at  $142\text{ cm}^{-1}$ , which corresponds to  $B_{1g}$  mode resulting from the symmetric bending vibration of O-Ti-O (Alhomoudi and Newaz 2009; Mulmi et al. 2016). Meanwhile, two dominant peaks observed at  $446$  and  $610\text{ cm}^{-1}$  resulted from O-Ti-O symmetric stretching vibration and anti-symmetric bending vibration, respectively (Yan et al. 2013). Conversely, the second-order scattering process featured the broad Raman peak located at  $236\text{ cm}^{-1}$ . These results confirmed the rutile phase of the fabricated  $\text{TiO}_2$  NRs (5 h) by the existence of three Raman active modes expressed as  $B_{1g} + E_g + A_{1g}$  (Alhomoudi and Newaz 2009; Danish et al. 2014; Hardcastle 2011; Mali et al. 2011; Mokhtar et al. 2018; Suriani et al. 2018b, 2018c). The additional weak peak observed at  $127\text{ cm}^{-1}$  represented quartz as an element of sand substrate (Sharma et al. 2006).

As the reaction time was prolonged, the intensity of two prominent peaks observed in the sand/ZnO NRs/ $\text{TiO}_2$  NRs (20 h) increased (red line graph). This result indicated that the sand/ZnO NRs/ $\text{TiO}_2$  NRs (20 h) possessed better crystallinity than the sand/ZnO NRs/ $\text{TiO}_2$  NRs (5 h) (Ahn et al. 2011; Mokhtar et al. 2018). Furthermore, these peaks blue-shifted to  $445$  and  $609\text{ cm}^{-1}$  in the  $E_g$  and  $A_{1g}$  modes, respectively, indicating that the  $\text{TiO}_2$  NRs (20 h) possessed larger crystallite size in the sand/ZnO NRs/ $\text{TiO}_2$  NRs (20 h) than in the sand/ZnO NRs/ $\text{TiO}_2$  NRs (5 h) (Li Bassi et al. 2005). Meanwhile, the multiple phonon scattering and  $B_{1g}$  mode were exhibited at  $236$  and  $142\text{ cm}^{-1}$ , respectively. These results further confirmed that the synthesized  $\text{TiO}_2$  NRs (20 h) were also in rutile phase (Liu et al. 2009; Ma et al. 2007; Woo et al. 2010). However, ZnO NRs peak was not detected in both nanocomposite samples because of its small content (Bai et al. 2013) in

the nanocomposites as presented in FESEM images and EDX analysis (Fig. 1a–f).

After the hybridization of GO and GO\_MWCNTs with sand/ZnO NRs/ $\text{TiO}_2$  NRs (5 h), two prominent peaks (D- and G-band) were clearly observed as shown in Fig. 2 (blue and green line graphs), indicating their existence in sand/ZnO NRs/ $\text{TiO}_2$  NRs (5 h). D-band was associated with the distortions and internal structural defects of carbon-based materials (Albert et al. 2018). Meanwhile, G-band was associated with  $E_{2g}$  vibrational mode, which resulted from the C-C bond in graphitic materials (Hosseini et al. 2018). The sand/ZnO NRs/ $\text{TiO}_2$  NRs (5 h)/GO and sand/ZnO NRs/ $\text{TiO}_2$  NRs (5 h)/GO\_MWCNTs presented the D-band at  $1400$  and  $1365\text{ cm}^{-1}$ , respectively, and the G-band at  $1588$  and  $1591\text{ cm}^{-1}$ , respectively. The blue-shift of the D-band on the sand/ZnO NRs/ $\text{TiO}_2$  NRs (5 h)/GO\_MWCNTs compared with the sand/ZnO NRs/ $\text{TiO}_2$  NRs (5 h)/GO indicated a good and strong interaction between GO and MWCNTs (Batakliiev et al. 2019; Suriani et al. 2019). Meanwhile, the red-shift of the G-band peak can be attributed to the dispersion and disentanglement of MWCNTs on the GO surface, which decreased the interaction between the MWCNTs (Batakliiev et al. 2019).

As shown in Fig. 2 (green line graph), the sand/ZnO NRs/ $\text{TiO}_2$  NRs (5 h)/GO\_MWCNTs also exhibited higher intensity in the D- and G-band peaks. The high intensity of D-band ( $I_D$ ) indicated high defect level, which means that the  $sp^2$  bonds were broken and formed new  $sp^3$  bonds (Bîru and Iovu 2018; Hodkiewicz 2010). Meanwhile, the high G-band intensity ( $I_G$ ) was associated with the strong compressive forces between GO and MWCNTs and well dispersion of the MWCNTs in the GO solution (Bokobza et al. 2008). Furthermore, the  $I_D/I_G$  ratio can be used to estimate the sample crystallinity, including the structural defect number, within the samples. The lower  $I_D/I_G$  ratio of the sand/ZnO NRs/ $\text{TiO}_2$  NRs (5 h)/GO\_MWCNTs (0.65) than the sand/ZnO NRs/ $\text{TiO}_2$  NRs (5 h)/GO (0.73) suggested lower structural defects, which can be ascribed to the incorporation of MWCNTs (Muda et al. 2017; Neelgund and Oki 2016). Furthermore, low structural defects suggested that the sand/ZnO NRs/ $\text{TiO}_2$  NRs (5 h)/GO\_MWCNTs possessed high structural and crystalline quality (Ivanova et al. 2012; Neelgund and Oki 2016; Srivastava et al. 2014; Wu et al. 2018). Moreover, the low  $I_D/I_G$  ratio observed in the sand/ZnO NRs/ $\text{TiO}_2$  NRs (5 h)/GO\_MWCNTs was due to the high amount of MWCNTs, indicating the good dispersion on the sand substrate (Batakliiev et al. 2019; Saner et al. 2013). The weak interaction between GO and MWCNTs also resulted lower  $I_D/I_G$  ratio in sand/ZnO NRs/ $\text{TiO}_2$  NRs (5 h)/GO\_MWCNTs sample (Zhang et al. 2010). This result can be supported by the FESEM images (Fig. 1j, k) where the formation of MWCNTs was dominant and well dispersed in the sand/

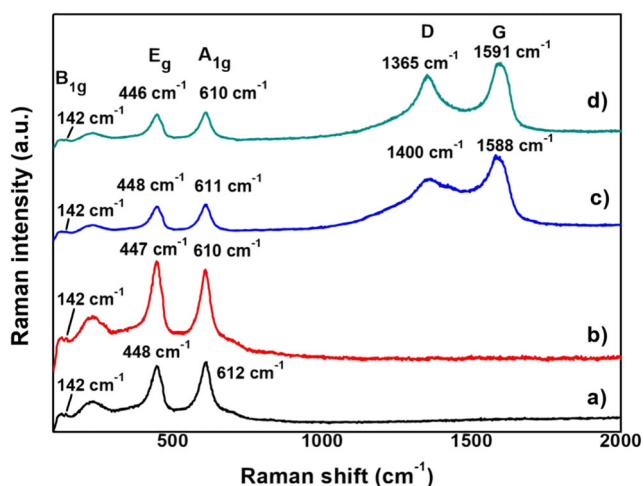


**Fig. 2** Micro-Raman spectra run at 514 nm wavelength of argon laser of sand/ZnO NRs/ $\text{TiO}_2$  NRs (5 h), sand/ZnO NRs/ $\text{TiO}_2$  NRs (20 h), sand/ZnO NRs/ $\text{TiO}_2$  NRs (5 h)/GO and sand/ZnO NRs/ $\text{TiO}_2$  NRs (5 h)/GO\_MWCNTs

ZnO NRs/TiO<sub>2</sub> NRs (5 h)/GO\_MWCNTs sample. Furthermore, other typical peaks at 142 (B<sub>1g</sub>), 237, 446 (E<sub>g</sub>) and 610 cm<sup>-1</sup> (E<sub>1g</sub>) represented the rutile phase of TiO<sub>2</sub>.

### UV-Vis spectroscopy

The photocatalytic activities of sand/ZnO NRs/TiO<sub>2</sub> NRs (5 and 20 h) nanocomposites, sand/ZnO NRs/TiO<sub>2</sub> NRs (5 h)/GO and sand/ZnO NRs/TiO<sub>2</sub> NRs (5 h)/GO\_MWCNTs nanohybrids were evaluated by measuring the degradation of 250 mL with 5 g/mL of MB solution under UV irradiation for 3 days (Fig. 3a). The photocatalytic performance of the sand/

ZnO NRs/TiO<sub>2</sub> NRs (20 h) (88.29% MB degradation) was weaker than that of the sand/ZnO NRs/TiO<sub>2</sub> NRs (5 h) (91.73%) after 3 days of measurement (Fig. 3b, c). This result was due to the decrement of ZnO NRs initial amount in the nanocomposite caused by the dissolution of ZnO in acid solution, which formed ZnCl<sub>2</sub>. Prolonged exposure of ZnO NRs to HCl increased the ZnO dissolution and thus decreased the number of active sites in the nanocomposite (Kalpana and Rajeswari 2018). This result can be supported by the FESEM images (Fig. 1d) where ZnO NRs were unobservable in the sand/ZnO NRs/TiO<sub>2</sub> NRs (20 h) sample. Given that it showed better photocatalytic performance than the sand/ZnO

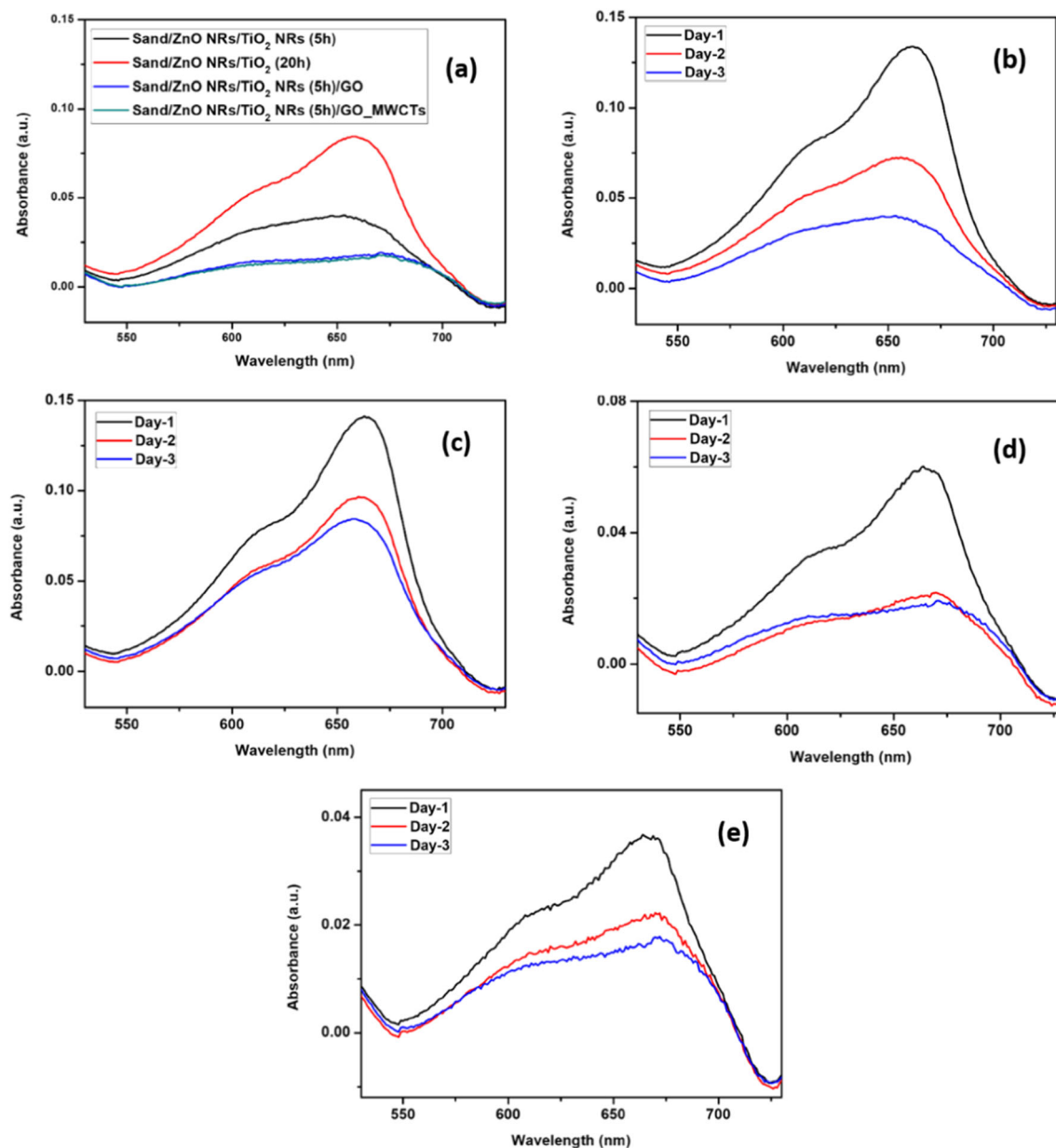


**Fig. 3** a UV-Vis absorption spectrum of the samples’ photocatalytic performance at day 3 and photocatalytic performance of b sand/ZnO NRs/TiO<sub>2</sub> NRs (5 h), c sand/ZnO NRs/TiO<sub>2</sub> NRs (20 h), d sand/ZnO

NRs/TiO<sub>2</sub> NRs (5 h)/GO and e sand/ZnO NRs/TiO<sub>2</sub> NRs (5 h)/GO\_MWCNTs within 3 days in the wavelength range of 200–800 nm



**Table 1** Percentage of MB removal for 3 days of sand/ZnO NRs/TiO<sub>2</sub> NRs (5 h), sand/ZnO NRs/TiO<sub>2</sub> NRs (20 h), sand/ZnO NRs/TiO<sub>2</sub> NRs (5 h)/GO and sand/ZnO NRs/TiO<sub>2</sub> NRs (5 h)/GO\_MWCNTs

Sample	Day 1 (%)	Day 2 (%)	Day 3 (%)
Sand/ZnO NRs/TiO <sub>2</sub> NRs (5 h)	87.24	90.21	91.73
Sand/ZnO NRs/TiO <sub>2</sub> NRs (20 h)	86.86	88.98	89.63
Sand/ZnO NRs/TiO <sub>2</sub> NRs (5 h)/GO	90.61	92.40	92.56
Sand/ZnO NRs/TiO <sub>2</sub> NRs (5 h)/GO_MWCNTs	91.68	92.39	92.60

NRs/TiO<sub>2</sub> NRs (20 h), the sand/ZnO NRs/TiO<sub>2</sub> NRs (5 h) sample was used for hybridization with carbon-based materials.

After the hybridization, the samples sand/ZnO NRs/TiO<sub>2</sub> NRs (5 h)/GO and sand/ZnO NRs/TiO<sub>2</sub> NRs (5 h)/GO\_MWCNTs showed similar MB degradation percentage after 3 days of measurement, which were 92.56% and 92.60%, respectively (Fig. 3a). These results also showed higher MB degradation percentage than the sand/ZnO NRs/TiO<sub>2</sub> NRs (5 h) (91.73%). This result was because most of the MB molecules were oxidized by the hydroxyl group or most of the active sites offered by both samples were occupied by MB molecules (Chen et al. 2017) at day 3. The higher MB degradation exhibited by the sand/ZnO NRs/TiO<sub>2</sub> NRs (5 h)/GO as compared with the sand/ZnO NRs/TiO<sub>2</sub> NRs (5 h) was due to the important role of GO as the electron transporter and acceptor in the nanocomposite owing to its 2D  $\pi$ -conjugation structure (Paul et al. 2017; Sharma et al. 2018; Wang et al. 2012).

The electrons from the sand/ZnO NRs/TiO<sub>2</sub> NRs (5 h) were transferred on the 2D planar structure of the GO nanosheets, which led to the prevention of the electron/hole recombination (Wang et al. 2012). Furthermore, GO with a large surface area acted as the charge carrier and transported the electrons to the photocatalyst surfaces to form reactive species and thus enhance the photocatalytic performance (Nenavathu et al. 2018; Raliya et al. 2017; Wang et al. 2012). This improvement was due to the further UV-light extension range that can be absorbed by the sand/ZnO NRs/TiO<sub>2</sub> NRs (5 h)/GO (Morales-torres and Martinez-Pastrana 2014; Pérez-Ramírez et al. 2016).

At day 3, the sand/ZnO NRs/TiO<sub>2</sub> NRs (5 h)/GO and sand/ZnO NRs/TiO<sub>2</sub> NRs (5 h)/GO\_MWCNTs exhibited similar MB degradation percentages. Thus, the comparison was made at day 1. The sand/ZnO NRs/TiO<sub>2</sub> NRs (5 h)/GO\_MWCNTs (91.68%) showed slightly higher MB degradation percentage than the sand/ZnO NRs/TiO<sub>2</sub> NRs (5 h)/GO (90.61%) (Fig. 3d, e). The MWCNTs possessed a unique tubular structure, which offered higher surface area with many active sites due to its 3D network and strong adsorption ability towards oxygen and water (Huang et al. 2018; Jiang et al. 2013). Compared with GO, the GO\_MWCNTs hybrid provided

larger surface area and promoted higher electron transfer, which could prolong the electron/hole separation and improve the effectiveness of dye adsorption capacity (Duan et al. 2016; Hosseini et al. 2018; Koay et al. 2016; Marco et al. 2017; Raliya et al. 2017; Saleh 2013; Shaban et al. 2018; Sui et al. 2012). As shown in Table 1, the MB degradation percentages for days 2 and 3 were not so obvious as that for day 1. This result was due to the fact that most of the active sites of all samples were occupied by dye molecules at day 1. Therefore, the photocatalytic performance was gradually decreasing for the next 2 days (Chen et al. 2017).

### Photocatalytic mechanism

The photocatalytic mechanism of sand/ZnO NRs/TiO<sub>2</sub> NRs (5 h)/GO\_MWCNTs nanohybrid begins when light energy in the form of photon strikes the surface of the photocatalyst with a greater or equal amount of energy to the band gap energy ( $E_g$ ). Electrons from valence band (VB) of ZnO NRs was excited to its conduction band (CB), which resulted in the generation of hole in the VB (Eq. 2). The electrons were then transferred to the TiO<sub>2</sub> NRs CB because TiO<sub>2</sub> NRs have lower  $E_g$  than ZnO NRs (Hellen et al. 2018). The electron transfers for the sand/ZnO NRs/TiO<sub>2</sub> NRs (5 and 20 h) nanocomposites were stopped at the TiO<sub>2</sub> NRs CB, which then fell back to the ZnO NRs VB and thus decreased the photocatalytic activity.

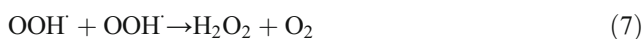


For the sand/ZnO NRs/TiO<sub>2</sub> NRs (5 h)/GO\_MWCNTs nanohybrid, the excited electron was then further transferred onto the surface of the GO\_MWCNTs hybrid. GO and MWCNTs exhibit rapid electron transfer because of their high electrical conductivity and high electron storage capacity, thereby preventing the accumulation of electrons and resulting in high electron mobilization (Chen et al. 2018; Ho et al. 2018; Hosseini et al. 2018; Kaur and Jeet 2017; Khan et al. 2012; Saleh 2013). The electrons moved freely along the conducting sheets and networks of GO and MWCNTs, respectively (Ahmad et al. 2018). This process inhibited the recombination rate of the electron and holes and thus enhanced the photocatalytic performance (Hosseini et al. 2018).

Meanwhile, the holes in the VB of the sand/ZnO NRs/TiO<sub>2</sub> NRs (5 h)/GO\_MWCNTs underwent oxidation, which reacted with absorbed water molecules and hydroxide ions (OH<sup>-</sup>) to generate hydroxyl radicals (OH<sup>•</sup>) (Eqs. 3 and 4). These radicals have an extremely strong oxidizing power that is responsible for MB dye degradation.

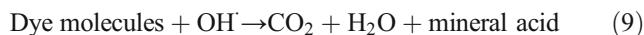


The transferred electron underwent reduction and reacted with the absorbed oxygen on the photocatalyst surface to form superoxide radical anions (e<sub>2</sub><sup>-</sup>). These (e<sub>2</sub><sup>-</sup>) can further react with H<sup>+</sup> to generate highly active hydrogen peroxide (H<sub>2</sub>O<sub>2</sub>). H<sub>2</sub>O<sub>2</sub> then dissociated into highly reactive OH<sup>•</sup> radicals. The electrons transferred in the reduction process are shown in Eqs. 5–8.



Therefore, the generated powerful and reactive hydroxyl radicals OH<sup>•</sup> oxidize the organic dye into CO<sub>2</sub> and H<sub>2</sub>O, which are harmless to the environment, as shown in Eq. 9. The GO\_MWCNTs hybrid in the sand/ZnO NRs/TiO<sub>2</sub> NRs (5 h)/GO\_MWCNTs nanohybrid provided a larger specific surface area and more active sites than the sand/ZnO NRs/TiO<sub>2</sub> NRs (5 and 20 h) nanocomposites and sand/ZnO NRs/TiO<sub>2</sub> NRs (5 h)/GO nanohybrid. Thus, an abundant number of hydroxyl groups formed on the surfaces. As a consequence, the

targeted MB molecules that were adsorbed can be oxidized on the surface of the sand/ZnO NRs/TiO<sub>2</sub> NRs (5 h)/GO\_MWCNTs and thus enhance the photocatalytic performance.



Moreover, the higher MB degradation possessed by the sand/ZnO NRs/TiO<sub>2</sub> NRs (5 h)/GO\_MWCNTs nanohybrid than the sand/ZnO NRs/TiO<sub>2</sub> NRs (5 h) nanocomposite was due to the higher adsorption of MB dye molecules onto the surface of sand/ZnO NRs/TiO<sub>2</sub> NRs (5 h)/GO\_MWCNTs photocatalysts by π-π interaction and oxygen functional groups offered by the GO\_MWCNTs hybrid (Ahmad et al. 2018; Thi et al. 2019; Vanitha et al. 2014; Zhang et al. 2014). An illustration of the photocatalytic mechanism is presented in Fig. 4.

### Conclusion

The sand/ZnO NRs/TiO<sub>2</sub> NRs-based photocatalysts were successfully fabricated via sol-gel immersion followed by a hydrothermal method. The sand/ZnO NRs/TiO<sub>2</sub> NRs (5 h)/GO\_MWCNTs presented the highest MB degradation removal (92.60%) after 3 days of measurement. This result was due to the utilization of the GO\_MWCNTs hybrid as an electron acceptor and transporter, which retarded the electron-hole recombination. Moreover, its large surface area allowed the formation of many active sites and hydroxyl ions on the surface. As a consequence, a large number of MB molecules were adsorbed on the surface and thus enhanced the photocatalytic performance. In conclusion, sand/ZnO NRs/TiO<sub>2</sub> NRs (5 h)/

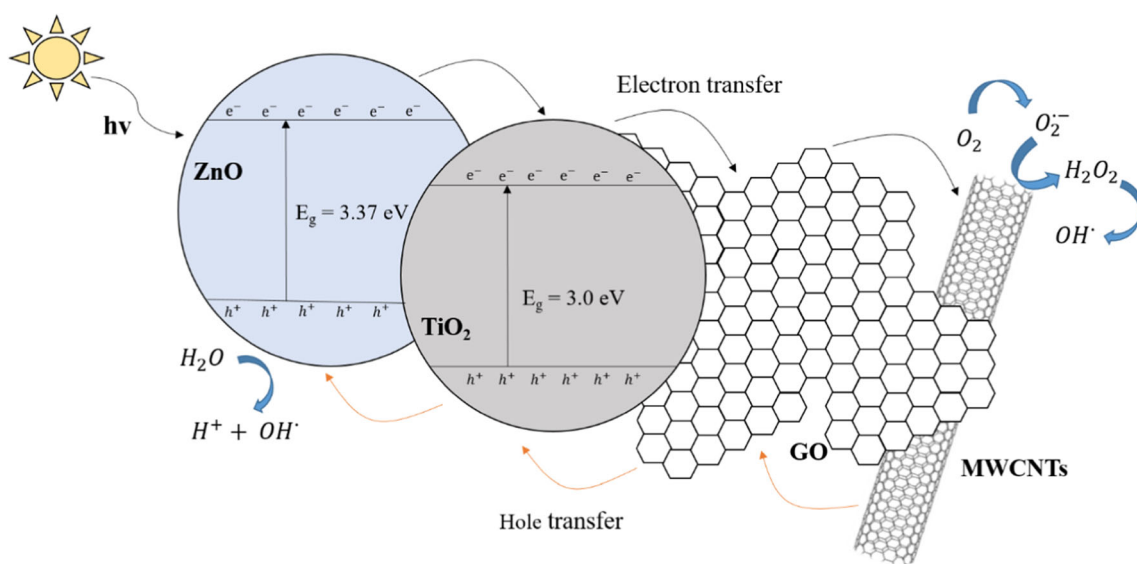


Fig. 4 Photocatalytic mechanism of sand/ZnO NRs/TiO<sub>2</sub> NRs (5 h)/GO\_MWCNTs nanohybrid photocatalyst

GO\_MWCNTs demonstrated a potential ability to be applied as a photocatalyst material to degrade MB solution. This study presented a simpler and low-cost production of sand/ZnO NRs/TiO<sub>2</sub> NRs-based photocatalysts materials for photocatalysis application. Further study could be done by increasing ZnO solution's molarity thus increased the amount of ZnO NRs growth. Moreover, the synthesis time of TiO<sub>2</sub> could be reduced thus resulted lower rate of ZnO NRs dissolution.

**Funding** The authors received financial support from the Fundamental Research Grand Scheme (grant no. 2015-0154-102-02).

## References

- Abdel-Maksoud YK, Imam E, Ramadan AR (2018) Sand supported TiO<sub>2</sub> photocatalyst in a tray photo-reactor for the removal of emerging contaminants in wastewater. *Catal Today* 313:55–62. <https://doi.org/10.1016/j.cattod.2017.10.029>
- Adnan MAM, Julkapli NM, Hamid SBA (2016) Review on ZnO hybrid photocatalyst: impact on photocatalytic activities of water pollutant degradation. *Inorg Chem* 36:1–28. <https://doi.org/10.1515/revic-2015-0015>
- Ahmad A, Razali MH, Mamat M, Kassim K, Amin KAM (2018) Physiochemical properties of TiO<sub>2</sub> nanoparticle loaded APTES-functionalized MWCNTs composites and their photocatalytic activity with kinetic study. *Arab J Chem* 13:2785–2794. <https://doi.org/10.1016/j.arabjc.2018.07.009>
- Ahn K, Lee HU, Jeong YM, Kim JP, Jeong SY, Cho CR (2011) Effects of TiO<sub>2</sub> nanorod length and post-annealing on the electrical properties of TiO<sub>2</sub> nanobarbed fiber structures. *J Nanosci Nanotechnol* 11(8):7155–7158
- Alansi AM, Alkayali WZ, Al-qunaibit Maha H et al (2015) Synthesis of exfoliated polystyrene/anionic clay MgAl-layered double hydroxide: structural and thermal properties. *RSC Adv* 5:71441–71448. <https://doi.org/10.1039/c5ra10545e>
- Albert EL, Che Abdullah CA, Shiroshaki Y (2018) Synthesis and characterization of graphene oxide functionalized with magnetic nanoparticle via simple emulsion method. *Results Phys* 11:944–950. <https://doi.org/10.1016/j.rinp.2018.10.054>
- Alhomoudi IA, Newaz G (2009) Residual stresses and Raman shift relation in anatase TiO<sub>2</sub> thin film. *Thin Solid Films* 517:4372–4378. <https://doi.org/10.1016/j.tsf.2009.02.141>
- Arthi G (2016) Investigation of growth and functional properties of TiO<sub>2</sub> nanostructures for dye sensitized solar cell applications. Dissertation, SRM Institute of Science and Technology, Chennai
- Azmina MS, Md Nor R, Rafeaie HA, Razak NSA, Sani SFA, Osman Z (2017) Enhanced photocatalytic activity of ZnO nanoparticles grown on porous silica microparticles. *Appl Nanosci* 7:885–892. <https://doi.org/10.1007/s13204-017-0626-3>
- Ba-abbad MM, Kadhum AAH, Mohamad AB, Takriff MS, Sopian K (2013) Optimization of process parameters using D-optimal design for synthesis of ZnO nanoparticles via sol-gel technique. *J Ind Eng Chem* 19:99–105. <https://doi.org/10.1016/j.jiec.2012.07.010>
- Bai LJ, Kou G, Gong ZY, Zhao ZM (2013) Effect of Zn and Ti mole ratio on microstructure and photocatalytic properties of magnetron sputtered TiO<sub>2</sub>-ZnO heterogeneous composite film. *Trans Nonferrous Metals Soc China (English Edition)* 23:3643–3649. [https://doi.org/10.1016/S1003-6326\(13\)62912-X](https://doi.org/10.1016/S1003-6326(13)62912-X)
- Banerjee S, Benjwal P, Singh M, Kar KK (2018) Graphene oxide (rGO)-metal oxide (TiO<sub>2</sub>/Fe<sub>3</sub>O<sub>4</sub>) based nanocomposites for the removal of methylene blue. *Appl Surf Sci* 439:560–568. <https://doi.org/10.1016/j.apsusc.2018.01.085>
- Basturk E, Karatas M (2015) Decolorization of antraquinone dye Reactive Blue 181 solution by UV/H<sub>2</sub>O<sub>2</sub> process. *J Photochem Photobiol A Chem* 299:67–72. <https://doi.org/10.1016/j.jphotochem.2014.11.003>
- Bataklijev T, Petrova-doycheva I, Angelov V et al (2019) Effects of graphene nanoplatelets and multiwall carbon nanotubes on the structure and mechanical properties of poly (acetic acid) composites. *Appl Sci* 9:469–473. <https://doi.org/10.3390/app9030469>
- Biru EI, Iovu H (2018) Graphene nanocomposites studied by Raman spectroscopy. In: Nascimento GMD (ed) Raman spectroscopy. IntechOpen, Brazil, pp 179–201
- Bodson CJ, Lambert SD, Alié C, Cattoën X, Pirard JP, Bied C, Man MWC, Heinrichs B (2010) Effects of additives and solvents on the gel formation rate and on the texture of P- and Si-doped TiO<sub>2</sub> materials. *Microporous Mesoporous Mater* 134:157–164. <https://doi.org/10.1016/j.micromeso.2010.05.021>
- Bokobza L, Rahmani M, Belin C, Bruneel JL, El Bounia NE (2008) Blends of carbon blacks and multiwall carbon nanotubes as reinforcing fillers for hydrocarbon rubbers. *J Polym Sci B Polym Phys* 46:1939–1951. <https://doi.org/10.1002/polb.21529>
- Brodie BC (1859) On the atomic weight of graphite. *J Storage* 149:249–259. <https://doi.org/10.1098/rstl.1859.0013>
- Chaudhary D, Singh S, Vankar VD, Khare N (2018) ZnO nanoparticles decorated multi-walled carbon nanotubes for enhanced photocatalytic and photoelectrochemical water splitting. *J Photochem Photobiol A Chem* 351:154–161. <https://doi.org/10.1016/j.jphotochem.2017.10.018>
- Chen X, Wu Z, Liu D, Gao Z (2017) Preparation of ZnO photocatalyst for the efficient and rapid photocatalytic degradation of azo dyes. *Nanoscale Res Lett* 12:143. <https://doi.org/10.1186/s11671-017-1904-4>
- Chen YF, Tan YJ, Li J, Hao YB, Shi YD, Wang M (2018) Graphene oxide-assisted dispersion of multi-walled carbon nanotubes in biodegradable Poly (ε-caprolactone) for mechanical and electrically conductive enhancement. *Polym Test* 65:387–397. <https://doi.org/10.1016/j.polymertesting.2017.12.019>
- Cheng C, Amini A, Zhu C, Xu Z, Song H, Wang N (2014) Enhanced photocatalytic performance of TiO<sub>2</sub>-ZnO hybrid nanostructures. *Sci Rep* 4:1–5. <https://doi.org/10.1038/srep04181>
- Cheng P, Wang Y, Xu L, Sun P, Su Z, Jin F, Liu F, Sun Y, Lu G (2016) High specific surface area urchin-like hierarchical ZnO-TiO<sub>2</sub> architectures: hydrothermal synthesis and photocatalytic properties. *Mater Lett* 175:52–55. <https://doi.org/10.1016/j.matlet.2016.03.120>
- Cirak BB, Caglar B, Kilinc T et al (2018) Synthesis and characterization of ZnO nanorice decorated TiO<sub>2</sub> nanotubes for enhanced photocatalytic activity. *Mater Res Bull* 109:160–167. <https://doi.org/10.1016/j.materresbull.2018.09.039>
- Da Dalt SD, Alves AK, Bergmann CP (2016) Preparation and performance of TiO<sub>2</sub>-ZnO/CNT hetero-nanostructures applied to photodegradation of organic dye. *Mater Res* 19:1372–1375. <https://doi.org/10.1590/1980-5373-mr-2016-0036>
- Danish R, Ahmed F, Arshi N, Anwar MS, Koo BH (2014) Facile synthesis of single-crystalline rutile TiO<sub>2</sub> nano-rods by solution method. *Trans Nonferrous Metals Soc China* 24:152–156. [https://doi.org/10.1016/S1003-6326\(14\)63303-3](https://doi.org/10.1016/S1003-6326(14)63303-3)
- Duan Q, Lee J, Liu Y, Qi H (2016) Preparation and photocatalytic performance of MWCNTs/TiO<sub>2</sub> nanocomposites for degradation of aqueous substrate. *J Chem* 2016:1–8. <https://doi.org/10.1155/2016/1262017>
- Eddy DR, Puri FN, Noviyanti AR (2015) Synthesis and photocatalytic activity of silica-based sand quartz as the supporting TiO<sub>2</sub> photocatalyst. *Procedia Chem* 17:55–58. <https://doi.org/10.1016/j.proche.2015.12.132>



- Fadillah G, Saleh TA, Wahyuningsih S (2019) Enhanced electrochemical degradation of 4-Nitrophenol molecules using novel Ti/TiO<sub>2</sub>-NiO electrodes. *J Mol Liq* 289:111108. <https://doi.org/10.1016/j.molliq.2019.111108>
- Fudzi ML, Zainal Z, Lim H, Chang SK, Holi A et al (2018) Effect of temperature and growth time on vertically aligned ZnO nanorods by simplified hydrothermal technique for photoelectrochemical cells. *Materials* 11(5):704. <https://doi.org/10.3390/ma11050704>
- Greenwood NN, Earnshaw A (1997) *Chemistry of elements*, 2nd edn. Elsevier, United Kingdom
- Habib MA, Shahadat MT, Bahadur NM, Ismail IMI, Mahmood AJ (2013) Synthesis and characterization of ZnO-TiO<sub>2</sub> nanocomposites and their application as photocatalysts. *Int Nano Lett* 3:1–8. <https://doi.org/10.1186/2228-5326-3-5>
- Hadjiltaief HB, Zina MB, Galvez ME, Costa PD (2016) Photocatalytic degradation of methyl green dye in aqueous solution over natural clay-supported ZnO-TiO<sub>2</sub> catalysts. *J Photochem Photobiol A Chem* 315:25–33. <https://doi.org/10.1016/j.jphotochem.2015.09.008>
- Hakki HK, Allahyari S, Rahemi N, Tasbihi M (2019) Surface properties, adherence, and photocatalytic activity of sol-gel dip-coated TiO<sub>2</sub>-ZnO films on glass plates. *Comptes Rendus Chimie* 22:393–405. <https://doi.org/10.1016/j.crci.2019.05.007>
- Hardcastle FD (2011) Raman spectroscopy of titania (TiO<sub>2</sub>) nanotubular water-splitting catalysts. *J Arkansas Acad Sci* 65:43–48
- Hellen N, Park H, Kim KN (2018) Characterization of ZnO/TiO<sub>2</sub> nanocomposites prepared via the sol-gel method. *J Korean Ceram Soc* 55:140–144. <https://doi.org/10.4191/kecers.2018.55.2.10>
- Ho KC, Teow YH, Mohammad AW, Ang WL, Lee PH (2018) Development of graphene oxide (GO)/multi-walled carbon nanotubes (MWCNTs) nanocomposite conductive membranes for electrically enhanced fouling mitigation. *J Membr Sci* 552:189–201. <https://doi.org/10.1016/j.memsci.2018.02.001>
- Hodkiewicz J (2010) Characterizing carbon materials with Raman spectroscopy. Thermo Fisher Scientific. <https://www.semanticscholar.org/paper/Characterizing-Carbon-Materials-with-Raman-Hodkiewicz/bd887f696e5f7305f0e77d8d0f2aa7b35942cbbd>. Accessed 15 Jan 2020
- Hosseini F, Kasaean A, Pourfayaz F, Sheikhpour M, Wen D (2018) Novel ZnO-Ag/MWCNT nanocomposite for the photocatalytic degradation of phenol. *Mater Sci Semicond Process* 83:175–185. <https://doi.org/10.1016/j.mssp.2018.04.042>
- Huang Y, Chen D, Hu X, Qian, Li D (2018) Preparation of TiO<sub>2</sub>/carbon nanotubes/reduced graphene oxide composites with enhanced photocatalytic activity for the degradation of Rhodamine B. *Nanomaterials* 8:1–9. <https://doi.org/10.3390/nano8060431>
- Hummers WS, Offeman RE (1957) Preparation of graphitic oxide. *Prepar Graphitic Oxide* 208:1937. <https://doi.org/10.1021/ja01539a017>
- Ivanova MV, Lamprecht C, Huzil JT, Foldvari M (2012) Pharmaceutical characterization of solid and dispersed carbon nanotubes as nanoexcipients. *Int J Nanomedicine* 7:403–415. <https://doi.org/10.2147/IJN.S27442>
- Jiang T, Zhang L, Ji M, Wang Q, Zhao Q, Fu X, Yin H (2013) Carbon nanotubes/TiO<sub>2</sub> nanotubes composite photocatalysts for efficient degradation of methyl orange dye. *Particuology* 11:737–742. <https://doi.org/10.1016/j.partic.2012.07.008>
- Kalpana VN, Rajeswari VD (2018) A review on green synthesis, biomedical applications, and toxicity studies of ZnO NPs. *Bioinorg Chem Appl* 201:1–12. <https://doi.org/10.1155/2018/3569758>
- Kaur K, Jeet K (2017) Electrical conductivity of water-based nanofluids prepared with graphene-carbon nanotube hybrid. *Fullerenes Nanotub Carbon Nanostruct* 25:726–734. <https://doi.org/10.1080/1536383x.2017.1389906>
- Katheresan V, Kansedo J, Lau SY (2018) Efficiency of various recent wastewater dye removal methods: a review. *J Environ Chem Eng* 6:4676–4697. <https://doi.org/10.1016/j.jece.2018.06.060>
- Khan Z, Chetia TR, Vardhaman AK, Barpuzary D, Sastri CV, Qureshi M (2012) Visible light assisted photocatalytic hydrogen generation and organic dye degradation by CdS-metal oxide hybrids in presence of graphene oxide. *RSC Adv* 2:12122–12128. <https://doi.org/10.1039/c2ra21596a>
- Khojasteh H, Salavati-Niasari M, Sangsefidi FS (2018) Photocatalytic evaluation of rGO/TiO<sub>2</sub> NWs/Pd-Ag nanocomposite as an improved catalyst for efficient dye degradation. *J Alloys Compd* 746:611–618. <https://doi.org/10.1016/j.jallcom.2018.02.345>
- Koay HW, Ruslinda AR, Hashwan SSB et al (2016) Surface morphology of reduced graphene oxide-carbon nanotubes hybrid film for bio-sensing applications. *IEEE Internatinal Conference on Semiconductors Electronics* 320–323. <https://doi.org/10.1109/smelec.2016.7573656>
- Kumar A, Madaria AR, Zhou C (2010) Growth of aligned single-crystalline rutile TiO<sub>2</sub> nanowires on arbitrary substrates and their application in dye-sensitized solar cells. *J Phys Chem C* 114:7787–7792. <https://doi.org/10.1021/jp100491h>
- Kumar SG, Rao KSRK (2015) Zinc oxide based photocatalysis: tailoring surface-bulk structure and related interfacial charge carrier dynamics for better environmental applications. *RSC Adv* 5:3306–3351. <https://doi.org/10.1039/c4ra13299h>
- Latthe SS, Gurav AB, Maruti CS, Vhatkar RS (2012) Recent progress in preparation of superhydrophobic surfaces: a review. *J Surface Eng Mater Adv Technol* 2:76–94. <https://doi.org/10.4236/jsemat.2012.22014>
- Li Bassi A, Cattaneo D, Russo V, Bottani CE, Barborini E, Mazza T, Piseri P, Milani P, Ernst FO, Wegner K, Pratsinis SE (2005) Raman spectroscopy characterization of titania nanoparticles produced by flame pyrolysis: the influence of size and stoichiometry. *J Appl Phys* 98:1–8. <https://doi.org/10.1063/1.2061894>
- Liu B, Aydil ES (2009) Growth of oriented single-crystalline rutile TiO<sub>2</sub> nanorods on transparent conducting substrates for dye-sensitized solar cells. *J Am Chem Soc* 131:3985–3990. <https://doi.org/10.1021/ja8078972>
- Liu P, Cai W, Fang M (2009) Room temperature synthesized rutile TiO<sub>2</sub> nanoparticles induced by laser ablation in liquid and their photocatalytic activity. *Nanotechnology* 20:285707–285713. <https://doi.org/10.1088/0957-4484/20/28/285707>
- Liu Y (2017) Application of graphene oxide in water treatment. *Earth Environ Sci* 94:1–7. <https://doi.org/10.1088/1755-1315/94/1/012060>
- Liu J, Wang Y, Ma J, Peng Y, Wang A (2018) A review on bidirectional analogies between the photocatalysis and antibacterial properties of ZnO. *J Alloys Compd* 783:898–918. <https://doi.org/10.1016/j.jallcom.2018.12.330>
- Ma HL, Yang JY, Dai Y, Zhang YB, Lu B, Ma GH (2007) Raman study of phase transformation of TiO<sub>2</sub> rutile single crystal irradiated by infrared femtosecond laser. *Appl Surf Sci* 253:7497–7500. <https://doi.org/10.1016/j.apsusc.2007.03.047>
- Malek MF, Mamat MH, Soga T, Rahman SA, Abu Bakar S, Ismail AS et al (2015) Thickness-controlled synthesis of vertically aligned c-axis oriented ZnO nanorod arrays: effect of growth time via novel dual sonication sol-gel process. *Jpn J Appl Phys* 55(1):15–21
- Mali SS, Shinde PS, Betty CA, Bhosale PN, Lee WJ, Patil PS (2011) Nanocoral architecture of TiO<sub>2</sub> by hydrothermal process: synthesis and characterization. *Applied Surface Science. Appl Surf Sci* 257:9737–9746. <https://doi.org/10.1016/j.apsusc.2011.05.119>
- Marco DM, Menzel R, Bawaked SM et al (2017) Hybrid effects in graphene oxide/carbon nanotube-supported layered double hydroxides: enhancing the CO<sub>2</sub> sorption properties. *Carbon* 123:616–627. <https://doi.org/10.1016/j.carbon.2017.07.094>
- Mauček D, Šuligoj A, Ristić A, Dražić G, Pintar A, Tušar NN (2018) Titania versus zinc oxide nanoparticles on mesoporous silica supports as photocatalysts for removal of dyes from wastewater at

- neutral pH. *Catal Today* 310:32–41. <https://doi.org/10.1016/j.cattod.2017.05.061>
- Mahmoodi NM (2013) Photocatalytic degradation of dyes using carbon nanotube and titania nanoparticle. *Water Air Soil Pollut* 224:1612–1619. <https://doi.org/10.1007/s11270-013-1612-3>
- Md Disa N, Abu Bakar S, Alfarisa S, Mohamed A, Md Isa I, Kamari A, Hashim N, Abd Aziz A, Rusop Mahmood M (2015) The synthesis of graphene oxide via electrochemical exfoliation method. *Adv Mater Res* 1109:55–59. <https://doi.org/10.4028/www.scientific.net/AMR.1109.55>
- Min C, Liu D, Shen C, Zhang Q, Song H, Li S, Shen X, Zhu M, Zhang K (2018) Unique synergistic effects of graphene oxide and carbon nanotube hybrids on the tribological properties of polyimide nanocomposites. *Tribol Int* 117:217–224
- Mokhtar SM, Ahmad MK, Soon SF et al (2018) Fabrication and characterization of rutile-phased titanium dioxide (TiO<sub>2</sub>) nanorods array with various reaction times using one step hydrothermal method. *Optik* 154:510–515. <https://doi.org/10.1016/j.ijleo.2017.10.091>
- Morales-torres S, Martinez-Pastrana LM (2014) Nanostructured carbon-TiO<sub>2</sub> photocatalysts for water purification: an overview. *Boletín del Grupo Español del Carbón* 32:19–14
- Muda MR, Ramli MM, Mat Isa SS, Halin DSC, Talip LFA, Mazelan NS, Anhar NAM, Dania NA (2017) Structural and morphological investigation for water-processed graphene oxide/single-walled carbon nanotubes hybrids. *Mater Sci Eng* 209:12030–12039. <https://doi.org/10.1088/1757-899X/209/1/012030>
- Mulmi DD, Thapa D, Dahal B, Baral D, Solanki PR (2016) Spectroscopic studies of boron doped titanium dioxide nanoparticles. *Int J Mater Sci Eng* 4:172–178. <https://doi.org/10.17706/ijmse.2016.4.3.172-178>
- Naknikham U, Boffa V, Magnacca G, Qiao A, Jensen LR, Yue Y (2017) Mutual-stabilization in chemically bonded graphene oxide–TiO<sub>2</sub> heterostructures synthesized by a sol–gel approach. *RSC Adv* 7:41217–41227. <https://doi.org/10.1039/c7ra07472g>
- Neelgund GM, Oki A (2016) Influence of carbon nanotubes and graphene nanosheets on photothermal effect of hydroxyapatite. *J Colloid Interface Sci* 484:135–145. <https://doi.org/10.1016/j.jcis.2016.07.078>
- Nenavathu BP, Kandula S, Verma S (2018) Visible-light-driven photocatalytic degradation of safranin-T dye using functionalized graphene oxide. *RSC Adv* 8:19659–19667. <https://doi.org/10.1039/C8RA02237B>
- Ong CB, Ng LY, Mohammad AW (2018) A review of ZnO nanoparticles as solar photocatalysts: synthesis, mechanisms and applications. *Renew Sust Energ Rev* 81:536–551. <https://doi.org/10.1016/j.rser.2017.08.020>
- Paul SSP, Radhika N, Borang O, Lydia IS, Merlin JP (2017) Visible light driven photodegradation of Rhodamine B using cysteine capped ZnO/GO nanocomposite as photocatalyst. *J Mater Sci Mater Electron* 28:6722–6730. <https://doi.org/10.1007/s10854-017-6367-y>
- Pérez-ramírez EE, Luz-asunción MD, Martínez-hernández AL, Velasco-santos C (2016) Graphene materials to remove organic pollutants and heavy metals from water: photocatalysis and adsorption. In: Cao W (ed) *Semiconductor photocatalysis: materials, mechanism and applications*. IntechOpen, China, pp 491–522
- Poorebrahimi S, Norouzbeigi R (2015) A facile solution-immersion process for the fabrication of superhydrophobic gibbsite films with a binary micro-nano structure: effective factors optimization via Taguchi method. *Appl Surf Sci* 356:157–166. <https://doi.org/10.1016/j.apsusc.2015.07.172>
- Prathan A, Sanglao J, Wang T, Bhoomanee C, Ruankham P, Gardchareon A, Wongrataphisan D (2020) Controlled structure and growth mechanism behind hydrothermal growth of TiO<sub>2</sub> nanorods. *Sci Rep* 10:1–11
- Qi K, Cheng B, Yu J, Ho W (2017) Review on the improvement of the photocatalytic and antibacterial activities of ZnO. *J Alloys Compd* 727:792–820. <https://doi.org/10.1016/j.jallcom.2017.08.142>
- Qiu J, Zhang P, Ling M, Li S, Liu P, Zhao H, Zhang S (2012) Photocatalytic synthesis of TiO<sub>2</sub> and reduced graphene oxide nanocomposite for lithium ion battery. *ACS Appl Mater Interfaces* 4:3636–3642. <https://doi.org/10.1021/am300722d>
- Raliya R, Avery C, Chakrabarti S, Biswas P (2017) Photocatalytic degradation of methyl orange dye by pristine titanium dioxide, zinc oxide, and graphene oxide nanostructures and their composites under visible light irradiation. *Appl Nanosci* 7:253–259. <https://doi.org/10.1007/s13204-017-0565-z>
- Ridhuan NS, Razak KA, Lockman Z, Aziz AA (2012) Structural and morphology of ZnO nanorods synthesized using ZnO seeded growth hydrothermal method and its properties as UV sensing. *PLoS One* 7:50405–50419
- Saleh TA (2011) The influence of treatment temperature on the acidity of MWCNT oxidized by HNO<sub>3</sub> or a mixture of HNO<sub>3</sub>/H<sub>2</sub>SO<sub>4</sub>. *Appl Surf Sci* 257:7746–7751. <https://doi.org/10.1016/j.apsusc.2011.04.020>
- Saleh TA (2013) The role of carbon nanotubes in enhancement of photocatalysis. In: *Syntheses and applications of carbon nanotubes and their composite*. Sotoru Suzuki, IntechOpen, pp 479–493
- Saleh TA (2015a) Nanocomposite of carbon nanotubes/silica nanoparticles and their use for adsorption of Pb(II): from surface properties to sorption mechanism. *Desalin Water Treat* 57:10730–10744. <https://doi.org/10.1080/19443994.2015.1036784>
- Saleh TA (2015b) Mercury sorption by silica/carbon nanotubes and silica/activated carbon: a comparison study. *J Water Supply Res Technol AQUA* 64(892–903):892–903. <https://doi.org/10.2166/aqua.2015.050>
- Saleh TA (2015c) Isotherm, kinetic, and thermodynamic studies on Hg(II) adsorption from aqueous solution by silica- multiwall carbon nanotubes. *Environ Sci Pollut Res* 22:16721–16731. <https://doi.org/10.1007/s11356-015-4866-z>
- Saleh TA (2020) Characterization, determination and elimination technologies for sulfur from petroleum: toward cleaner fuel and a safe environment. *Trends Environ Anal Chem* 25:e00080. <https://doi.org/10.1016/j.teac.2020.e00080>
- Saner B, Gürsel SA, Yürüm Y (2013) Layer-by-layer polypyrrole coated graphite oxide and graphene nanosheets as catalyst support materials for fuel cells. *Fullerenes Nanotub Carbon Nanostruct* 21:233–247. <https://doi.org/10.1080/1536383X.2011.613536>
- Saravanan R, Gracia F, Stephen A (2017) Basic principles, mechanism, and challenges of photocatalysis. *Springer Series on Polymer and Composite Materials*, 19–40. [https://doi.org/10.1007/978-3-319-62446-4\\_2](https://doi.org/10.1007/978-3-319-62446-4_2)
- Shaban M, Ashraf AM, Abukhadra MR (2018) TiO<sub>2</sub> nanoribbons/carbon nanotubes composite with enhanced photocatalytic activity; fabrication, characterization, and application. *Sci Rep* 8:1–17. <https://doi.org/10.1038/s41598-018-19172-w>
- Shahriary L, Ghourchian H, Athawale AA (2014) Graphene-multiwalled carbon nanotube hybrids synthesized by gamma radiations: application as a glucose sensor. *J Nanotechnol* 2014:1–10. <https://doi.org/10.1155/2014/903872>
- Shan AY, Ghazi TIM, Rashid SA (2010) Immobilisation of titanium dioxide onto supporting materials in heterogeneous photocatalysis: a review. *Appl Catal A Gen* 389:1–8. <https://doi.org/10.1016/j.apsusc.2010.08.053>
- Sharma M, Behl K, Nigam S, Joshi M (2018) TiO<sub>2</sub>-GO nanocomposite for energy and environmental applications: a green synthesis approach. *Vacuum* 156:434–439. <https://doi.org/10.1016/j.vacuum.2018.08.009>
- Sharma SK, Misra AK, Ismail S, Singh UN (2006) Remote Raman spectroscopy of various MIXED and composite mineral phases at 7.2 m distance. NASA Technical Report Server, 1-2.

- Siwińska-Stefańska K, Kubiak A, Piasecki A, Goscińska J, Nowaczyk G, Jurga S, Jesionowski T (2018) TiO<sub>2</sub>-ZnO binary oxide systems: comprehensive characterization and tests of photocatalytic activity. *Materials* 11:841–859. <https://doi.org/10.3390/ma11050841>
- Siwińska-Stefańska K, Kubiak A, Piasecki A, Dobrowolska A, Czarczyk K, Motylenko M, Rafaja D, Ehrlich H, Jesionowski T (2019) Hydrothermal synthesis of multifunctional TiO<sub>2</sub>-ZnO oxide systems with desired antibacterial and photocatalytic properties. *Appl Surf Sci* 463:791–801. <https://doi.org/10.1016/j.apsusc.2018.08.256>
- Srivastava RK, Xingjue W, Kumar V, Srivastava A, Singh V (2014) Synthesis of benzimidazole-grafted graphene oxide/multi-walled carbon nanotubes composite for supercapacitance application. *J Alloys Compd* 612:343–348. <https://doi.org/10.1016/j.jallcom.2014.05.214>
- Sui Z, Meng Q, Zhang X, Ma R, Cao B (2012) Green synthesis of carbon nanotube-graphene hybrid aerogels and their use as versatile agents for water purification. *J Mater Chem* 22:8767–8771. <https://doi.org/10.1039/C2JM00055E>
- Sun N, Ma J, Wang C, Xue J, Qiang L, Tang J (2018) A facile and efficient method to directly synthesize TiO<sub>2</sub>/rGO with enhanced photocatalytic performance. *Superlattice Microst* 121:1–8. <https://doi.org/10.1016/j.spmi.2018.07.017>
- Suriani AB, Norhafizah J, Mohamed A, Mamat MH, Malek MF, Ahmad MK (2016) Scaled-up prototype of carbon nanotube production system utilizing waste cooking palm oil precursor and its nanocomposite application as supercapacitor electrodes. *J Mater Sci Mater Electron* 27:11599–11605. <https://doi.org/10.1007/s10854-016-5291-x>
- Suriani AB, Fatiatun MA et al (2018a) Reduced graphene oxide/platinum hybrid counter electrode assisted by custom-made triple-tail surfactant and zinc oxide/titanium dioxide bilayer nanocomposite photoanode for enhancement of DSSCs photovoltaic performance. *Optik* 161:70–83. <https://doi.org/10.1016/j.ijleo.2018.02.013>
- Suriani AB, Fatiatun MA et al (2019) Improved DSSC photovoltaic performance using reduced graphene oxide-carbon nanotube/platinum assisted with customised triple-tail surfactant as counter electrode and zinc oxide nanowire/titanium dioxide nanoparticle bilayer nanocomposite as photoanode. *Graphene Technol* 4:17–31. <https://doi.org/10.1007/s41127-019-00024-x>
- Suriani AB, Muqoyyanah MA et al (2018b) Improving the photovoltaic performance of DSSCs using a combination of mixed-phase TiO<sub>2</sub> nanostructure photoanode and agglomerated free reduced graphene oxide counter electrode assisted with hyperbranched surfactant. *Optik* 158:522–534. <https://doi.org/10.1016/j.ijleo.2017.12.149>
- Suriani AB, Muqoyyanah MA et al (2018c) Reduced graphene oxide-multiwalled carbon nanotubes hybrid film with low Pt loading as counter electrode for improved photovoltaic performance of dye-sensitised solar cells. *J Mater Sci Mater Electron* 29:10723–10743. <https://doi.org/10.1007/s10854-018-9139-4>
- Tayel A, Ramadan A, El Seoud O (2018) Titanium dioxide/graphene and titanium dioxide/graphene oxide nanocomposites: synthesis, characterization and photocatalytic applications for water decontamination. *Catalysts* 8:491–535. <https://doi.org/10.3390/catal8110491>
- Thi T, Ha V, Pham TN, Pham TT, Le MC (2019) Synergistic adsorption and photocatalytic activity under visible irradiation using Ag-ZnO/GO nanoparticles derived at low temperature. *J Chem* 2019:1–13
- Vanitha M, Keerthi Vadivel S, Balasubramanian N (2014) Visible light photocatalysis of Methylene blue by graphene-based ZnO and Ag/AgCl nanocomposites. *Desalin Water Treat* 54:2748–2756. <https://doi.org/10.1080/19443994.2014.903207>
- Wang J, Tsuzuki T, Tang B, Hou X, Sun L, Wang X (2012) Reduced graphene oxide/ZnO composite: reusable adsorbent for pollutant management. *Appl Mater Interfaces* 4:3084–3090. <https://doi.org/10.1021/am300445f>
- Wei A, Sun XW, Xu CX, Dong ZL, Yang Y, Tan ST, Huang W (2006) Growth mechanism of tubular ZnO formed in aqueous solution. *Nanotechnology* 17:1740–1744. <https://doi.org/10.1088/0957-4484/17/6/033>
- Wetchakun K, Wetchakun N, Sakulsermsuk S (2019) An overview of solar/visible light-driven heterogeneous photocatalysis for water purification: TiO<sub>2</sub>- and ZnO-based photocatalysts used in suspension photoreactors. *J Ind Eng Chem* 71:19–49. <https://doi.org/10.1016/j.jiec.2018.11.025>
- Woo H, Sung H, Gil H, Chan J, Young D (2010) Growth, structural, raman, and photoluminescence properties of rutile TiO<sub>2</sub> nanowires synthesized by the simple thermal treatment. *J Alloys Compd* 504(1):217–223. <https://doi.org/10.1016/j.jallcom.2010.05.094>
- Wu K, Wu B, Li C, Hu X (2018) Gradation, dispersion, and tribological behaviors of nanometric diamond particles in lubricating oils. In: Davim J (ed) *Introduction to mechanical engineering*. Springer, Portugal, pp 113–133
- Wu W, Zhang C, Hou S (2017) Electrochemical exfoliation of graphene and graphene-analogous 2D nanosheets. *J Mater Sci* 52:10649–10660. <https://doi.org/10.1007/s10853-017-1289-x>
- Yan J, Wu G, Guan N, Li L, Li Z, Cao X (2013) Understanding the effect of surface/bulk defects on the photocatalytic activity of TiO<sub>2</sub>: anatase versus rutile. *Phys Chem Chem Phys* 15:10978–10988. <https://doi.org/10.1039/C3CP50927C>
- Yu P, Lowe SE, Simon GP, Zhong YL (2015) Electrochemical exfoliation of graphite and production of functional graphene. *Curr Opin Colloid Interface Sci* 20:329–338. <https://doi.org/10.1016/j.cocis.2015.10.007>
- Yu S, Wang X, Zhang R, Yang T, Ai Y, Wen T, Huang W, Hayat T, Alsaedi A, Wang X (2017) Complex roles of solution chemistry on graphene oxide coagulation onto titanium dioxide: batch experiments, spectroscopy analysis and theoretical calculation. *Sci Rep* 7:39625–39635. <https://doi.org/10.1038/srep39625>
- Zhang L, Du L, Yu X et al (2014) Significantly enhanced photocatalytic activities and charge separation mechanism of Pd-decorated ZnO-graphene oxide nanocomposites. *ACS Appl Mater Interfaces* 6:3623–3629. <https://doi.org/10.1021/am405872r>
- Zhang Y, Wu B, Xu H, Liu H, Wang M, He Y, Pan B (2016) Nanomaterials-enabled water and wastewater treatment. *Nanoimpact* 3–4:22–39. <https://doi.org/10.1016/j.impact.2016.09.004>
- Zhang C, Ren L, Wang X, Liu T (2010) Graphene oxide-assisted dispersion of pristine multiwalled carbon nanotubes in aqueous media. *J Phys Chem C* 114:11435–11440. <https://doi.org/10.1021/jp103745g>

**Publisher's note** Springer Nature remains neutral with regard to jurisdictional claims in published maps and institutional affiliations.